Hindawi
Advances in Civil Engineering
Volume 2018, Article ID 2934302, 11 pages
https://doi.org/10.1155/2018/2934302

Research Article

Physical Modeling of Displacement and Failure Monitoring of Underground Roadway in Horizontal Strata

Dinggui Hou[1,2] **and Xiaojie Yang**[3,4]

[1]*Construction Engineering Department, North China Institute of Aerospace Engineering, Langfang 065000, China*
[2]*School of Civil and Environmental Engineering, University of Science and Technology Beijing, Beijing 100083, China*
[3]*State Key Laboratory for Geo-Mechanics and Deep Underground Engineering, China University of Mining and Technology, Beijing 100083, China*
[4]*School of Mechanics and Civil Engineering, China University of Mining and Technology, Beijing 100083, China*

Correspondence should be addressed to Dinggui Hou; houdinggui@126.com

Received 12 September 2017; Revised 6 March 2018; Accepted 20 March 2018; Published 16 May 2018

Academic Editor: Arnaud Perrot

Physical modeling of the underground roadway in horizontal strata is carried out by using a newly developed physical modeling approach, the so-called "physically finite elemental slab assemblage (PFESA)." The numerical 2D digital image correlation (DIC) technology is used to carry out the real-time monitoring of the surface displacement of the model in the experimental process, and the axial force monitoring devices called the small bolt (SB) and small constant resistance bolt (SCRB) are designed for the real-time detection of the roadway mechanics data. The displacement information of the whole physical model experiment process is obtained through the DIC technology. The SCRB can be well used to the mechanical monitoring of the deformation and failure of the roadway, though the analysis of the displacement and mechanical monitoring data can get that the change of the mechanical monitoring data of SCRB in advance of the displacement, the information of instability destruction precursor in roadway surrounding rock is the continuous increase of mechanical monitoring value in a short time. The experiment provides reference for the stability monitoring and early warning of the roadway surrounding rock based on a constant resistance and large deformation rock bolt (CRLB).

1. Introduction

Coal resources accounted for about 70% of China's energy consumption. More than 90% of the total output is obtained by underground mining, but the mining condition is bad, and the coal resources mining depth increases 8–12 meters every year; over the next 20 years, most of the coal mine in China will enter the 1000–1500 meters mining depth. The environment of deep mining is very complex; this caused the coal mine safety accident rate to be higher and accurately grasped the status and development trend of the surrounding rock through monitoring and early warning, which is very important for the security of coal mine production.

The stability problem of the roadway surrounding rock is studied by many experts: Ma et al. [1], Shen et al. [2], Zhang et al. [3], Fekete et al. [4], Cohe et al. [5], Fraldi and Guarracino [6], Eberhardt [7], Li et al. [8], Lai et al. [9], and Małkowski [10], by adopting the method of physical model for the study of the issue. The influence of the structural plane and the main structural surface has not been considered in these existing experiments, but these are abundant in the engineering rock mass; at the same time, the displacement and strain of the large-scale physical model are measured by the method of arrangement of the strain monitoring point, and it is difficult to realize the large deformation measurement of the physical model.

At present, the main technology for roadway surrounding rock condition monitoring is deformation monitoring, microseismic monitoring, electromagnetic radiation monitoring, bolt stress monitoring, and so on which are studied by Trifu et al. [11], Brady and Leighton [12], Kent et al. [13], Phillips et al. [14], Tan et al. [15], Yang et al. [16],

Table 1: Mechanical parameters of the engineering rock mass.

Group	Volume weight (kN/m^3)	Compressive strength (MPa)	Tensile strength (MPa)	Elastic modulus (GPa)	Poisson's ratio	Cohesive strength (MPa)	Internal friction angle (°)
Diabase	28.47	102.74	8.72	20.24	0.32	32	57
Green schist	27.45	46.96	4.57	16.82	0.18	7.7	54
Coal	18.29	14.82	0.37	7.20	0.21	0.48	48

Table 2: Mechanical parameters of the physically finite elemental slab assemblage.

Group	Unit size (cm)	Water-gypsum ratio	Volume weight (kN/m^3)	Compressive strength (MPa)	Tensile strength (MPa)	Elastic modulus (GPa)	Poisson's ratio
Diabase	$40 \times 40 \times 3$	0.8 : 1	10.45	9.58	0.99	3.35	0.12
Green schist	$40 \times 40 \times 2$	1 : 1	9.83	5.50	0.54	2.02	0.24
Coal	$40 \times 40 \times 1$	1.2 : 1	7.46	2.14	0.22	0.75	0.35

Lian et al. [17], and so on, by adopting the method of field application for the study of the issue, but the accuracy of the monitoring and early warning of roadway surrounding rock stability needs to be improved.

The physical model is constructed by the "physically finite elemental slab assemblage (PFESA)," the structural plane in which the rock stratum is considered. The numerical 2D digital image correlation (DIC) technology is used to carry out the real-time monitoring of the surface displacement of the model. Aiming at the problems existing in the stability monitoring of the surrounding rock of the roadway, a small constant resistance bolt (SCRB) is designed with the mechanical and geometric similarity ratio of the constant resistance bolt, and the SCRB is built in the physical model for the monitoring of the mechanical information during the experiment.

2. Physical Model Construction

2.1. Rock Model Material. Da Tai coal mine is the experimental engineering geological background, and the physical and mechanical parameters of the surrounding rock of the tunnel can be obtained from the field and indoor physical mechanics experiment, as shown in Table 1.

Conventionally, the construction of a large-scale geological model is very expensive and difficult to operate. To overcome these problems, a new approach, that is, the PFESA, initially proposed by He Manchao, was used for the construction of large-scale physical models to mimic stratified layers with different inclinations. This PFESA method uses a specimen-sized rectangular plate, that is, the elemental slab, made of artificial materials similar to the real rocks in terms of the physical and mechanical properties. The elemental slabs can be put into mass production at a low cost. Large numbers of these elemental slabs are arranged, making layers at specified orientations in the simulation of these strata. The elemental slabs were made of similar materials, that is, gypsum and water. The ratio of water to gypsum was obtained according to the test of rock specimens. After testing, the elemental slabs can be recycled and repeatedly used. Hence, large-scale physical models can be constructed conveniently at lower costs [18, 19].

Samples were taken from the surrounding rock masses in the roadway in the Da Tai coal mine. The geometric and physical parameters for the elemental slabs are presented in Table 2. The dimensions of the elemental slabs are 400 mm × 400 mm × 10/20/30 mm. A large number of these elemental slabs were assembled in layers with different mechanical properties, simulating the rock strata of the coal seam, diabase, and green schist of the real rock masses. The rock layers were arranged at a zero dip angle with respect to the horizontal structure in order to mimic the horizontally distributed strata in the real rock in the test conducted in our investigation.

2.2. Rock Strata. Figure 1 shows the principle for producing rock strata. A large number of the elementary slabs (shown in Figure 1(b)) with the same model rock property were used to ensemble a rock layer of the same property, and a certain number of the rock layers with the same rock property were used to construct a rock stratum. As shown schematically in Figure 1(a), the green schist stratum and coal seam stratum are assembled by placing the elementary slabs in layers with perfectly mated interfaces. A weak surface is formed between the two different model rock strata. This weak surface is homogeneous along its striking at a macroscopic scale, while it has many minor asperities at a "microscopic scale" constituted by many small gaps between the parallel-placed elemental slabs in the rock layer. The gaps and asperities formed by the layered slabs also exist within the rock strata. These minor flaws can be viewed as the origin of the heterogeneity of the rock under external loading. Three classes of the model rock strata were constructed in our test, that is, diabase stratum, green schist stratum, and coal stratum which create two types of interfaces or weak faces, that is, green schist-coal interface and diabase-coal interface.

2.3. Geological Model. The large-scale physical model was built with a total of six strata including one diabase, three green schists, and two coal seams, and all the strata are inclined at an angle of 0° with respect to the horizontal structure, to simulate near horizontal geological structures. The constructed geological model, as shown schematically in

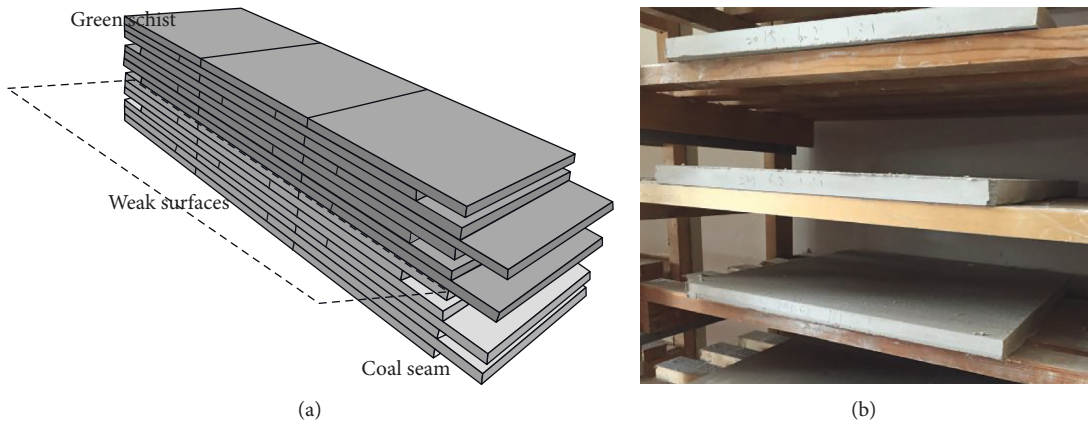

Figure 1: Weak bedding surface of the rock strata simulated by the similar materials; (a) schematic of the rock strata and their interface; (b) photograph of the gypsum boards.

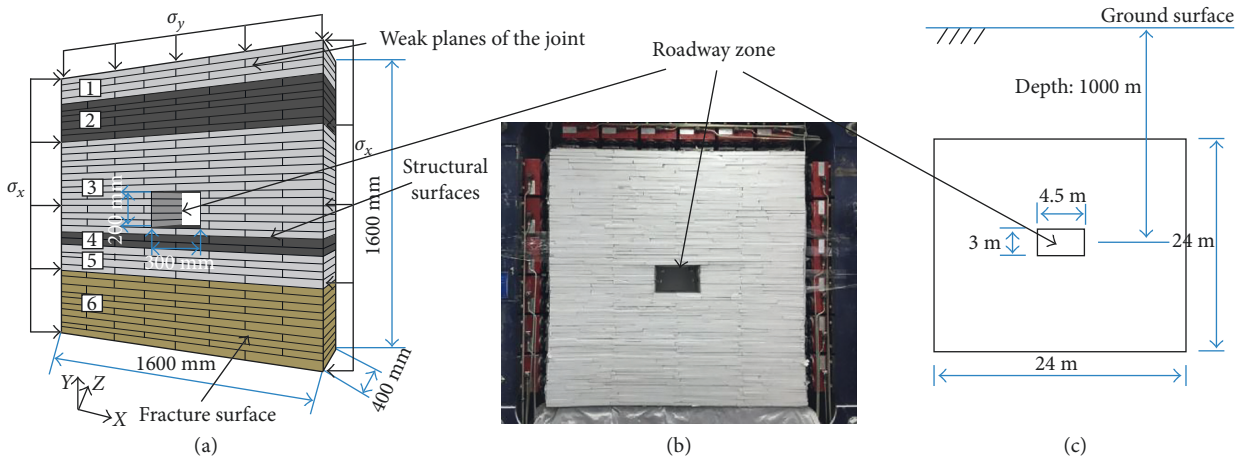

Figure 2: Physical model design: (a) schematic of the model; (b) photograph of the model; (c) rock reality of the deep underground roadway simulated by the gypsum board.

Figure 2(a), is 1600 mm high, 1600 mm wide, and 40 mm thick. According to the size of the surrounding rock loose circle and the model loading system, the geometric similarity ratio is $C_l = 15$ and the size of the roadway of the model has a length 300 mm and the height 200 mm. According to the maximum load set degree of the model and the mechanical parameters of the engineering rock mass, the similarity coefficient of stress is $C_\sigma = 9$, the similarity coefficient of density is $C_\rho = 9/15 = 0.6$, and the physical model is shown in Figure 2. The alternating strata are indexed with 1–6 from top to bottom with the geological profile, and geometric parameters of the physical model are shown in Table 3.

Table 3: Geological section, material, and structural parameters of the physical model from top to bottom.

Number	Lithology	Thickness (mm)	Legend	Number of plies
1	Green schist	180		400 × 400 × 20
2	Coal	220		400 × 400 × 10
3	Green schist	560		400 × 400 × 20
4	Coal	80		400 × 400 × 10
5	Green schist	160		400 × 400 × 20
6	Diabase	400		400 × 400 × 20

3. Monitoring of the Physical Model

3.1. Digital Image Correlation. The digital image correlation (DIC) is a no-contact displacement-strain measurement technique, which is also called the digital speckle correlation method (DSCM), and the image measurement is realized based on the computer vision technology. Through noncontact means, the full-field displacement and strain measurement can be achieved.

The DIC technique has obvious advantages compared with the contact-type displacement and strain measurement. Through real-time monitoring of surface displacement, the displacement and strain information of the measured object surface can be obtained, collected, and extracted.

The MTI-2D digital image correlation measurement system is shown in Figure 3. The system mainly includes the image acquisition system, lighting system, and digital image

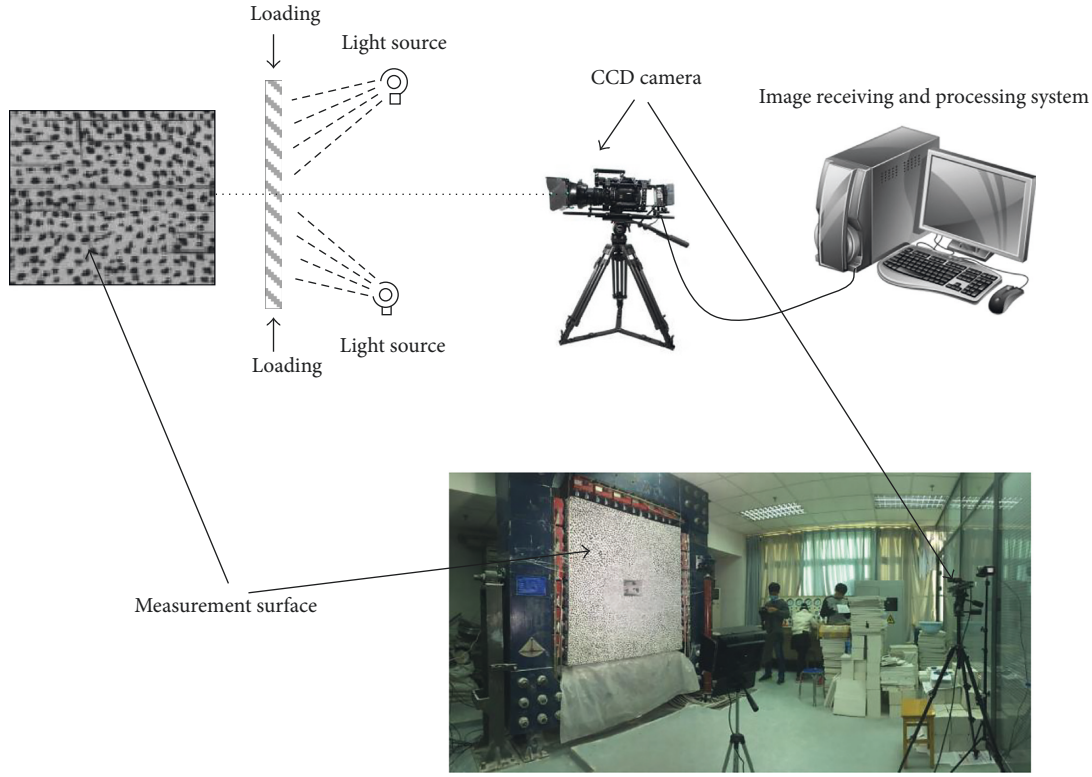

Figure 3: Diagrammatic sketch of the DIC system.

processing system. In the experiment, the common white light can be used as the light source, and the illumination system can be added to ensure that the uniform light field is formed on the surface of the test piece. In order to obtain the accurate deformation image, the CCD camera is placed on the precision three-dimensional support and is made parallel to the surface of the specimen. Image acquired is directly deposited onto the image card and imported into the computer. Image saving format can be of BMP or tiff format. In the image analysis step, the image extracted will be saved for further analysis.

3.2. SCRB Monitoring. With the increase of mining depth, the failure of roadways often has the characteristics of large nonlinear deformation. Under the mining conditions such as mining disturbance and high pressure, the traditional small deformation rock bolts can only bear the deformation of the roadway surrounding rock within 200 mm and cannot adapt to the large deformation and failure characteristics of the surrounding rock of the deep roadway; therefore, in roadway support projects, it often appears that the bolt cannot adapt to the large deformation and tensile failure of the surrounding rock, resulting in the tunnel collapse and roof fall accident.

In view of the disadvantage of the small deformation of the bolt in the deep roadway support, domestic and foreign scholars have conducted studies on the tensile strength of bolts and achieved fruitful results. The energy-absorbing bolt can provide constant support resistance in the roadway creep stage and provide a large amount of extension. The mechanical characteristics, structural characteristics, and working mechanism of several typical bolts are analyzed by Professor He MC, and a new type of an energy-absorbing anchor rod is developed which is called the constant resistance and large deformation bolt (CRLB).

Through a large number of laboratory experiments and the engineering field experimental studies, the CRLB can also provide a constant support resistance in the process of deformation. The structure of the CRLB includes the nut, the ball pad, the tray, the constant resistance device, and the rod body. The constant resistance device can provide deformation and constant resistance; the tray and the nut are arranged at the tail part of the constant resistance device, and the constant resistance device is connected with the nut through the screw thread. CRLB is shown in Figure 4.

The constant resistance device is the main component of the CRLB to ensure the constant resistance of the device, and its design strength is 80%–90% of the anchor rod body. When the surrounding rock deformation is large, CRLB resistance can be kept constant and the deformation energy of the surrounding rock can be absorbed by CRLD; hence, CRLD can still play a good supporting effect when the surrounding rock is under large deformation state.

A small constant resistance large deformation bolt (SCRB) is developed, which is suitable for indoor physical model experiments. The supporting structure used in the experiment only considers the similarity of mechanics and geometry. According to the similarity theory of the physical model, the geometric similarity ratio of the bolt is $C_l = 15$, which is used to calculate the length and diameter of the anchor rod in the physical model. The mechanical similarity

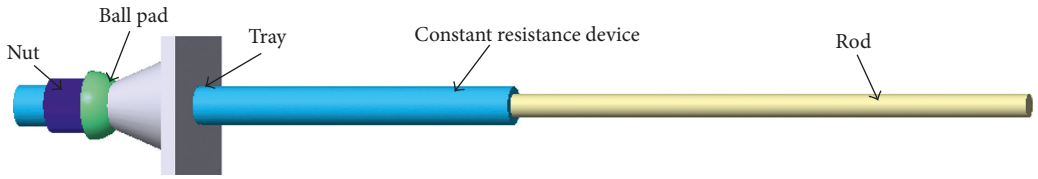

Figure 4: Sketch map of the constant resistance and large deformation bolt.

Table 4: Prototype and model physical and mechanical parameters of the bolt.

Bolt type		Load value (N)	Pretightening force (N)	Length (m)	Diameter (cm)
Bolt in roof	Prototype parameters	500000	150000	6	1.2
	Parameters in the model	247.0	74.1	0.4	0.05
Bolt on both sides	Prototype parameters	160000	50000	4	00.8
	Parameters in the model	79.0	24.7	0.27	0.05

Figure 5: Diagram of the small-sized constant resistance and large deformation bolt.

ratio is $C_F = C_\rho C_l^3 = 0.6 \times 15^3 = 2025$, which can be used for the calculation of bolt preload and tensile load.

The ordinary small bolt (SB) supports similar materials of physical model experiments as shown in Table 4. The SCRB is composed of rod and constant resistance device; the constant resistance device meet the mechanical and geometric similar ratio, and it can provide 40 mm deformation. The constant resistance device is assembled by tray and round tube; the outer diameter of the round tube is 60 mm, and the thickness is 2.5 mm. The deformation length of the SCRB can be adjusted by setting the length of the constant resistance device; in this paper, the constant resistance value of the constant resistance is 90% of the strength of the rod body. The diagram of SCRB is shown in Figure 5.

With reference to the situation of roadway support in Da Tai coal mine, the arrangement of SCRB and SB monitoring devices is shown in Figure 6. The constant resistance device and anchor rod body and pull pressure sensor are assembled into the SCRB monitoring device, and the layout and number of the bolts are shown in Table 5.

4. Analysis of Experimental Results

4.1. Loading Path and Experimental Process. The loading path is derived from the measurement and calculation results of in situ stress, and the load and stress similarity ratio is also set by in situ detection and measurement. The vertical and horizontal stress of the roadway can be obtained. The horizontal and vertical direction of the model tunnel is loaded according to the stress similarity ratio. The different levels of model boundary load calculations are as follows:

$$\sigma_x = \frac{\sigma_h}{C_\sigma},$$
$$\sigma_y = \frac{\sigma_v}{C_\sigma}, \quad (1)$$

where σ_x is the horizontal stress boundary, σ_y is the vertical stress boundary, σ_v is the weight of the different depth of stress, σ_h is the horizontal stress, and C_σ is the stress similarity ratio.

The loading process of the model experiment is designed for four stages: A–D, by applying σ_x and σ_y realization. The loading process and the loading path are shown in Figure 7. The horizontal stress and vertical stress increase at the same time during the A stage, and the horizontal stress remains unchanged; the vertical stress increases at the B stage, and the vertical stress remains unchanged; the horizontal stress increases at the C stage; the horizontal stress and vertical stress increase at the same time at the D stage.

At stage A, the horizontal and vertical stresses increase to 0.2 MPa. After 4 times of loading, 0.8 MPa stress is achieved, and each loading time is for 30 minutes; at this stage, the gaps between PFESAs are closed. At stage B, the horizontal stress (0.8 MPa) remains unchanged. After 10 times of loading, the vertical stress of 2.8 MPa is achieved, and each loading time is 30 minutes. The loading increases 0.2 MPa each time. Then, at the C loading stage, the vertical stress remains unchanged, the horizontal stress is increased from

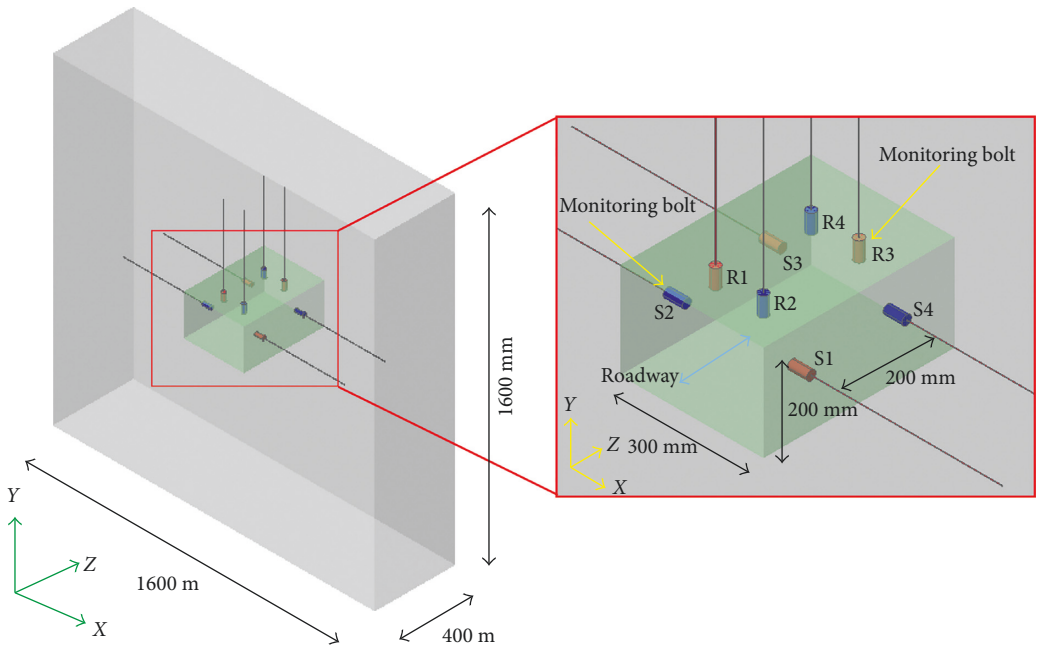

Figure 6: Schematic diagram of the physical model of the monitoring bolt device arrangement.

Table 5: Layout and number of monitoring bolt devices.

Layout position	Number	Type	Length of the bolt (mm)	Length of the constant resistance device (mm)	Load value (N)	Constant resistance value (N)
Bolt in roof	R1	Constant resistance bolt	400	40	247.0	222.3
	R2	Traditional bolt	400	0	247.0	No
	R3	Constant resistance bolt	400	40	247.0	222.3
	R4	Traditional bolt	400	0	247.0	No
Bolt on both sides	S1	Constant resistance bolt	270	40	79.0	71.1
	S2	Traditional bolt	270	0	79.0	No
	S3	Constant resistance bolt	270	40	79.0	71.1
	S4	Traditional bolt	270	0	79.0	No

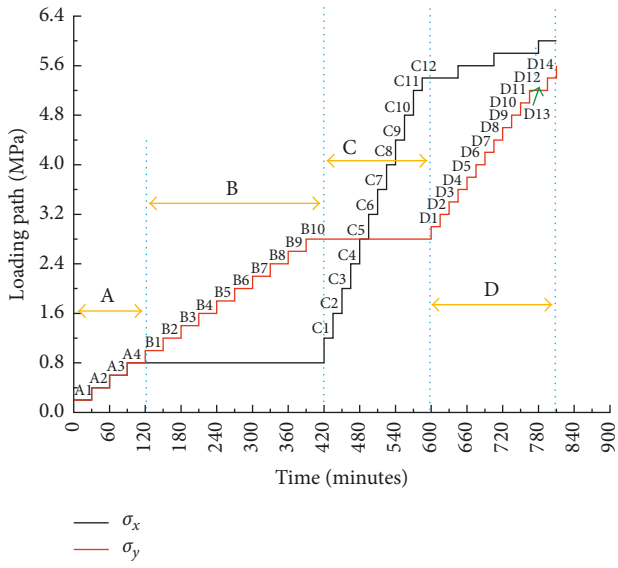

Figure 7: Loading scheme of the physical model.

1.2 MPa to 5.4 MPa, and each loading time is 15 minutes. The loading increases 0.4 MPa each time. At the end of the C loading stage, the horizontal and vertical stresses reach the stress condition of roadway at −510 m. The final stage is the D loading stage; at this stage, the vertical load stress increases from 3.0 MPa to 5.6 MPa, and the horizontal stress increases from 5.4 MPa to 6 MPa.

4.2. Model Failure Process

4.2.1. Vertical Displacement Field. Through the digital image acquisition and processing in the model experiment, the evolution characteristics of the whole vertical displacement field of the physical model can be obtained as shown in Figure 8.

During stage A, the downward vertical displacement value has been in a state of growth, and in the A4 stage, the maximum vertical downward displacement value is 27.65 mm. With the increase of the vertical load, the vertical displacement value increases; when the value of the vertical load reaches 1.4 MPa, the maximum vertical displacement value is about 31.50 mm.

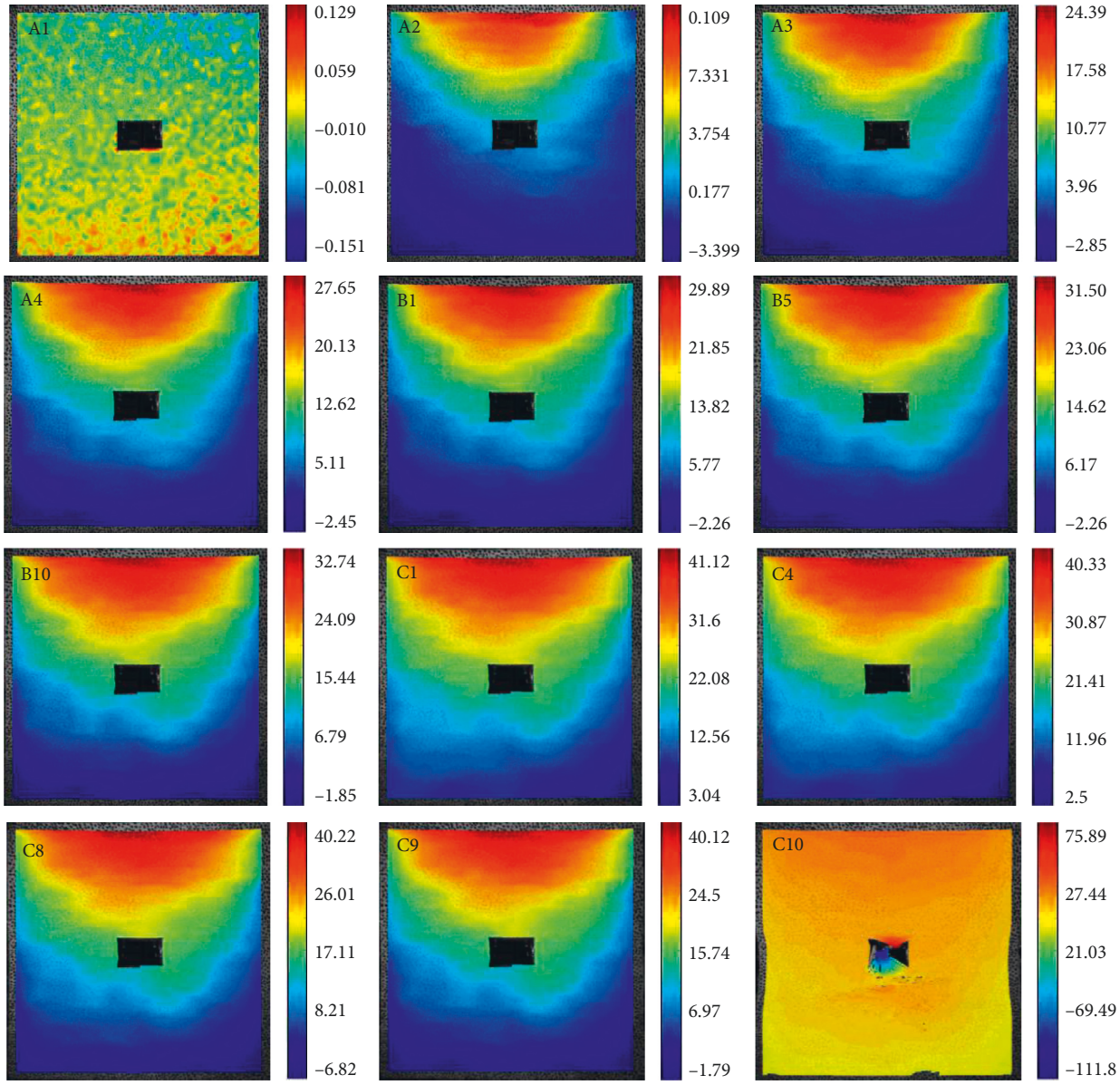

Figure 8: Evolution of the vertical displacement field (mm).

The vertical load during the B3~B10 stages is increased from 1.4 MPa to 2.8 MPa, and the vertical displacement is basically unchanged and is between −1.85 mm and 32.74 mm.

At the C1 stage, the vertical load (2.8 MPa) remains unchanged and the horizontal load increases; there is a rapid increase of the vertical displacement, and the maximum vertical displacement is about 32 mm to 40 mm, which remains basically in the stable state in the C1~C8 stage vertical displacement.

During the C9 stage, the horizontal load is 2.8 MPa, the vertical load is 4.4 MPa, the model of this stage begins to break down, the bottom drum and roof fall off, the bottom heave value is 111.8 mm, and the roof falls down 75.89 mm.

4.2.2. Horizontal Displacement Field. Through the DIC in the model experiment, the evolution characteristics of the whole horizontal displacement field of the physical model can be obtained as shown in Figure 9.

From the graph, we can see that, during the A1-A2 loading stage, the horizontal displacement rapidly generates after loading and the value is about 4 mm–12 mm; the displacement region is concentrated on two sides of the roadway model at the A3–B10 stage, mainly when the vertical load is applied, and the horizontal displacement is smaller in magnitude.

When the vertical load of 2.8 MPa is applied, at the C1 stage, the horizontal load began to increase, and the model produces about 10 mm–22 mm left displacement, until the C8 stage, the distance of the roadway on the right side is about 2.69 mm and the left side is 8.72 mm.

At the C9 loading stage, the horizontal load value is 4.4 MPa, the vertical load value is 2.8 MPa, the final distance

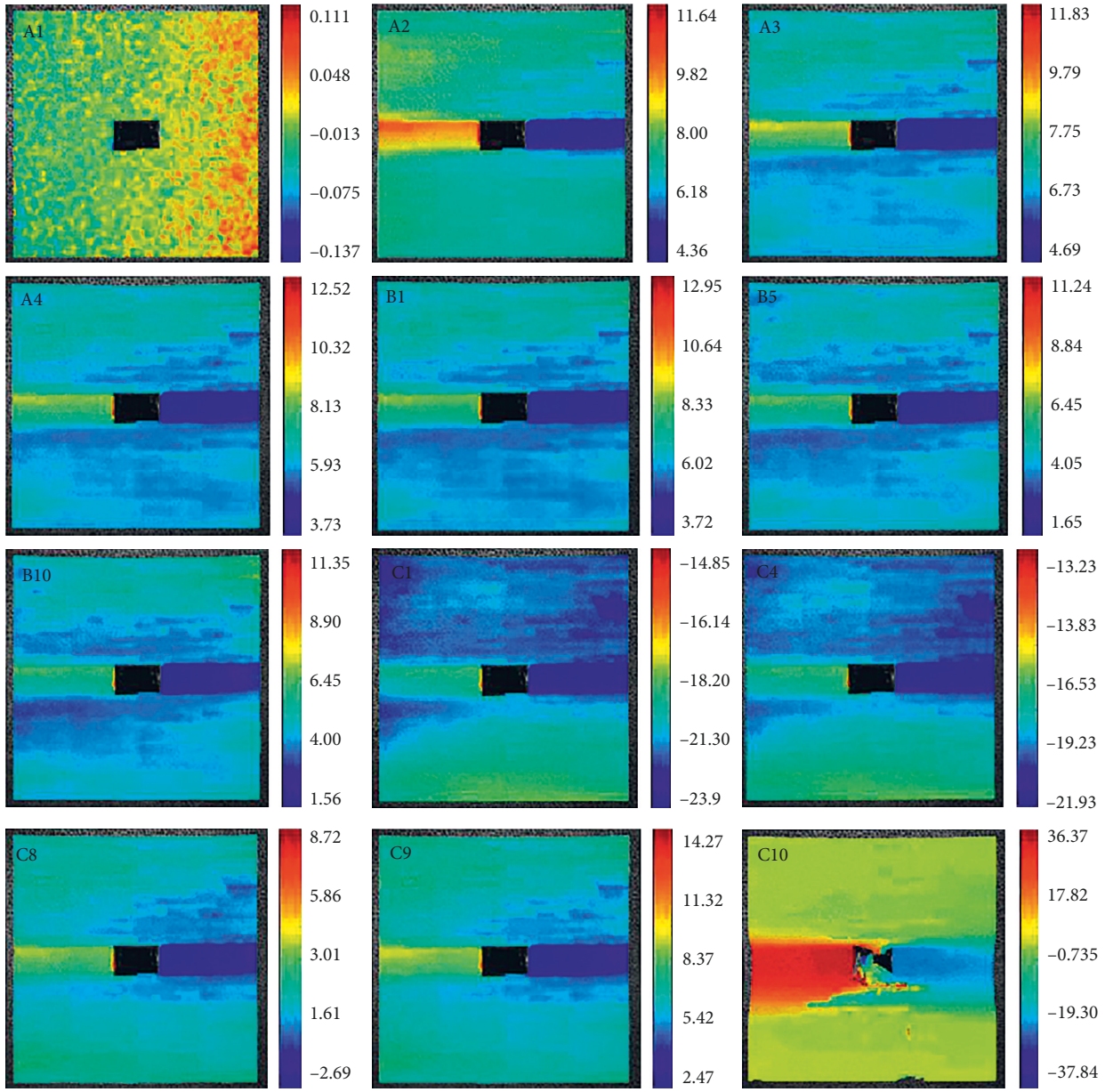

Figure 9: Evolution of the horizontal displacement field (mm).

of the roadway on the left side is about 36.37 mm, and on the right side, it moves 37.84 mm away.

4.3. Stress Monitoring of the Rock Bolt. In the course of the experiment, curves of bolt axial force with time are obtained as shown in Figure 10. The roof and two sides monitoring bolts are arranged as shown in Figure 6, in which R1 and R3 are SCRB monitoring devices and R2 and R4 are SB monitoring devices. From the curves, it can be obtained that, during the A1–A4 loading stages, the bolt axial force monitoring curve of the roof continued to rise. During B1–B10 loading stages, the monitoring curve slows down, and from the C loading stage, the monitoring curve rises rapidly. R2 and R4 monitoring curves in the axial force peak decreased dramatically after that in the roadway deformation and failure process because the force has exceeded its capacity, the rod body occurrence pulled, and failure occurred. R1 and R3 monitoring curves, respectively, maintain 220 N and 230 N stress, until the complete model failure. The SCRB can withstand the constant resistance monitoring of the surrounding rock and will not break until the roadway is completely destructed, and the SCRB monitoring device can monitor the whole failure process of the roadway.

The monitoring curve of bolt axial force on two sides of the roadway is shown in Figure 11, in which S1 and S3 are SCRB monitoring curves and S2 and S4 are SB monitoring curves. In the deformation and failure mode, the roadway is dominated by the roof floor heave and roof falling; therefore, the two-side roadway has less stress, resulting in the small bolt force value, and the bolt force did not exceed the load limit.

Through analysis of the monitoring curve, we conclude that the SCRB monitoring device can realize the whole

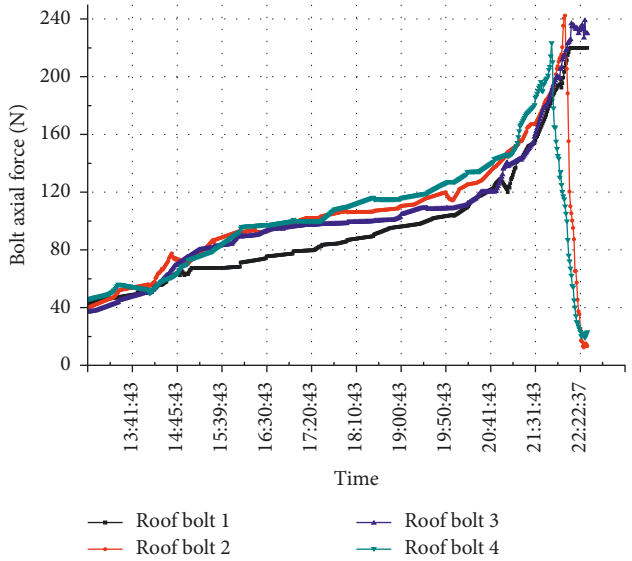

Figure 10: Bolt axial force-time curve of the roadway roof.

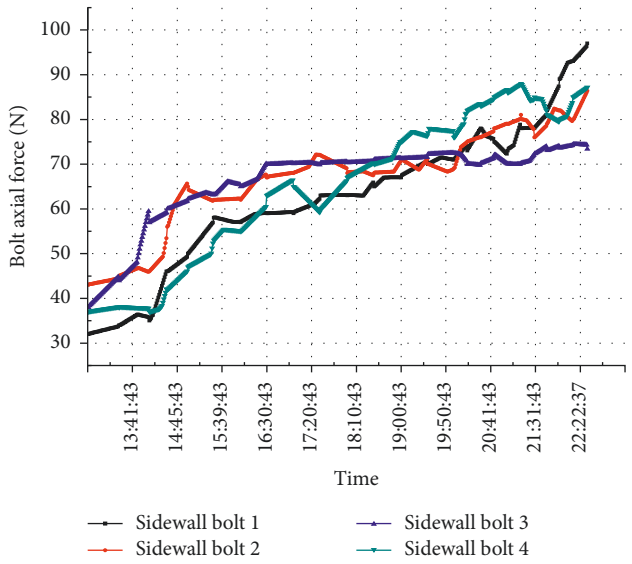

Figure 11: Bolt axial force-time curve of the two-side roadway.

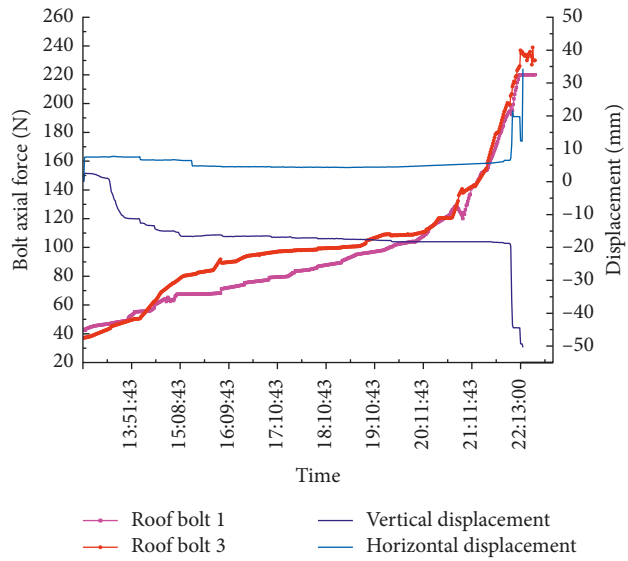

Figure 12: Displacement-time curve of the left side roadway.

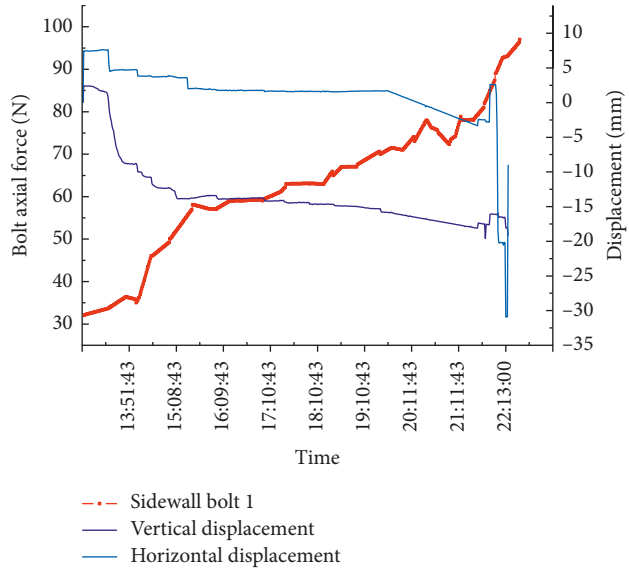

Figure 13: Displacement-time curve of the right side roadway.

process monitoring of the roadway deformation and failure. In the experiment, deformation and failure of the roadway mainly occurred on the roof and floor; two sides destroy model is overall launch, so the force monitoring effect of the two sides is poor.

4.4. Stress and Deformation Monitoring. Figure 12 is the axial force monitoring curve of R1 and R3 bolts and is the roof horizontal displacement and vertical displacement monitoring curve at the same time period. During the loading phase B, the roof displacement remained unchanged, and the bolt stress kept slowly rising. At C5 loading stage, the roadway cracks of the model began to develop, the bolt axial force also began to accelerate, and the roof displacement is still unchanged. From the C9 loading stage, the roadway began to destroy; at this time, the horizontal displacement and vertical displacement of the moment changed. By the analysis of the acceleration of the axial force of the bolt, it is found that it can be used as the precursor information of the failure of the model roadway.

Figures 13 and 14 are the S1 and S3 axial force monitoring curves and the displacement monitoring curves at the corresponding position. From the figures, we can see that the force value before and after the deformation and failure of the roadway has not reached its extreme value, which is caused by the failure of the roadway; after the model failure, the force curves have a rising trend, but the force monitoring effect is not obvious compared to the roof bolt.

R1 and R3 have the best warning effect, the bolt axial force monitoring curves have experienced the slow rising stage and the accelerated phase, and the acceleration stage

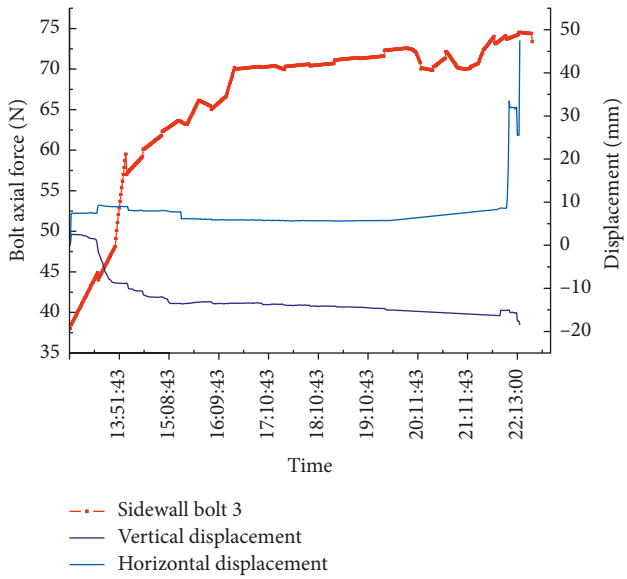

Figure 14: Displacement-time curve of the left side roadway.

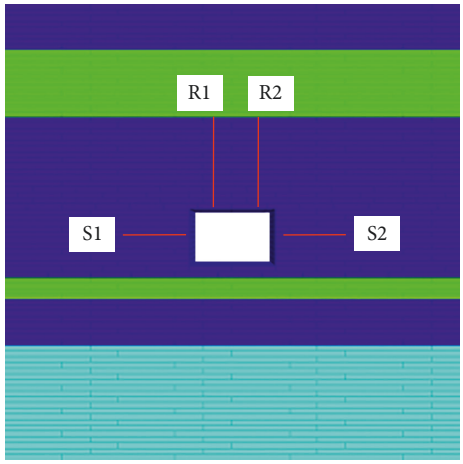

Figure 15: Numerical simulation model.

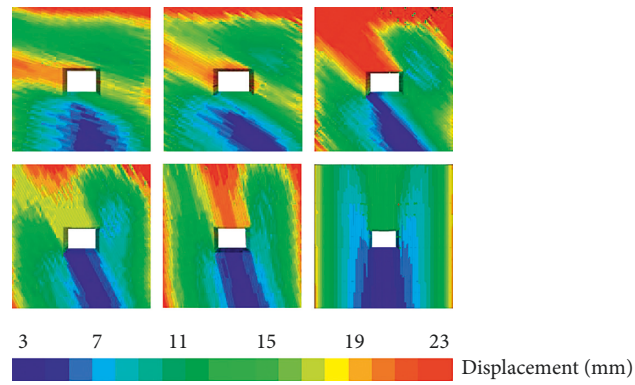

Figure 16: Displacement distribution of the different rock inclination model.

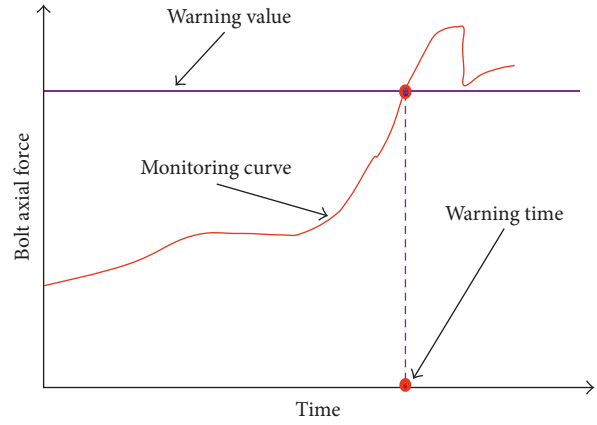

Figure 17: Characters of monitoring curves of the roadway instability mode.

can be used as the information of the early warning stage for the deformation and failure of the roadway.

5. Numerical Simulation Verification

To validate the model experiment, the discrete element method is used to simulate the same conditions but different rock inclination angles. The numerical model of the dip rock stratum at 15, 30, 45, 60, 75, and 90 degrees is established, and the force of the bolt and the displacement of the surrounding rock are monitored. The SCRB monitoring devices are numbered R1, R2, S1, and S2, and the numerical model is shown in Figure 15.

The displacement field of different rock inclination angles is simulated as shown in Figure 16; therefore, the deformation and failure of the roadway surrounding rock are significantly affected by rock inclination. The failure of the roadway surrounding rock is caused by large asymmetric deformation, and the instability model is dominated by shear slip in the key part.

The monitoring effect of the monitoring bolt is affected by the distribution of the roadway failure area, and the monitoring effect in key parts of the surrounding rock is better. When arranging the monitoring bolt, the failure field distribution of the surrounding rock should be taken into full consideration.

Through the physical model experiment and numerical simulation of different rock inclination angles, the monitoring value of the SCRB monitoring device is 0.7-0.8 times of its constant resistance. The characteristic changes of the mechanical monitoring curve of the SCRB monitoring device is shown in Figure 17. The monitoring curve has a significant ascending stage; when it reaches the warning value, the corresponding time is the warning time; when the monitoring curve exceeds the warning value to the maximum value, the roadway surrounding rock failure occurs.

6. Conclusion

Aiming at the problem of monitoring and early warning of the stability of the surrounding rock of the layered roadway, the monitoring technology of surrounding rock stability of the roadway based on the CRLB is put forward. According

to the similarity theory, the SCRB is developed which can be applied to the indoor physical model experiment, and SB and SCRB monitoring devices are built into the physical model body. Through the physical model experiment and numerical simulation, the following conclusions are obtained:

(1) The SCRB can withstand large deformation of roadway failure, and the whole process of monitoring roadway deformation destruction can be achieved, while the SB found it difficult to realize the roadway deformation and failure, which is the drawback of the whole process of monitoring and early warning.

(2) The force monitoring curves of the SCRB are in an accelerating stage before the large deformation and failure of the roadway, and then the curve rises to a certain value after the roadway deformation and failure; so the accelerated phase of the monitoring curve can be used as the early warning information of the roadway surrounding rock.

(3) Numerical simulations verify the correctness of the physical model experimental results, and the monitoring value of the SCRB monitoring device is 0.7-0.8 times its constant resistance.

Conflicts of Interest

The authors declare that they have no conflicts of interest.

Acknowledgments

Financial support from the Beijing Natural Science Foundation under Grant no. 8142032 and the Independent Selection Key Research Project of the State Key Laboratory for Geo-Mechanics and Deep Underground Engineering under Grant no. GDUEZB201404 is gratefully acknowledged.

References

[1] S. P. Ma, X. H. Xu, and Y. H. Zhao, "Geo-DSCM system and its application to deformation measurement of rock mechanics," *International Journal of Rock Mechanics and Mining Sciences*, vol. 41, no. 3, pp. 411-412, 2004.

[2] B. Shen, A. King, and H. Guo, "Displacement, stress and seismicity in roadway roofs during mining-induced failure," *International Journal of Rock Mechanics and Mining Sciences*, vol. 45, no. 5, pp. 672–688, 2008.

[3] Q. Y. Zhang, X. G. Chen, B. Lin, D. J. Liu, and N. Zhang, "Study of 3D geomechanical model test of zonal disintegration of surrounding rock of deep tunnel," *Chinese Journal of Rock Mechanics and Engineering*, vol. 28, no. 9, pp. 1757–1766, 2009, in Chinese.

[4] S. Fekete, M. Diederichs, and M. Lato, "Geotechnical and operational applications for 3-dimensional laser scanning in drill and blast tunnels," *Tunnelling and Underground Space Technology*, vol. 25, no. 5, pp. 614–628, 2010.

[5] T. Cohe, R. Masri, and D. Durban, "Analysis of circular hole expansion with generalized yield criteria," *International Journal of Solids and Structures*, vol. 46, no. 20, pp. 3643–3650, 2009.

[6] M. Fraldi and F. Guarracino, "Analytical solution for collapse mechanisms in tunnels with arbitrary cross sections," *International Journal of Solids and Structures*, vol. 47, no. 2, pp. 216–223, 2010.

[7] E. Eberhardt, "Numerical modelling of three-dimension stress rotation ahead of an advancing tunnel face," *International Journal of Rock Mechanics and Mining Sciences*, vol. 38, no. 4, pp. 499–518, 2001.

[8] S. C. Li, D. C. Wang, Q. Wang et al., "Development and application of large scale geomechanical model test system for deep thick topcoal roadway," *Journal of China Coal Society*, vol. 38, no. 9, pp. 1522–1530, 2013, in Chinese.

[9] X. P. Lai, P. F. Shan, J. W. Deng, J. T. Cao, F. Cui, and C. L. Wang, "Physical simulation on strata behavior of large mining height fully mechanized face in shallow-buried and thick seam," *Journal of Mining and Safety Engineering*, vol. 31, no. 3, pp. 418–423, 2014, in Chinese.

[10] P. Małkowski, "The impact of the physical model selection and rock mass stratification on the results of numerical calculations of the state of rock mass deformation around the roadways," *Tunnelling and Underground Space Technology*, vol. 50, pp. 365–375, 2015.

[11] C. Trifu, T. Urbancic, and R. P. Young, "Source parameters of mining-induced seismic events: an evaluation of homogeneous and inhomogeneous faulting models for assessing damage potential," *Pure and Applied Geophysics*, vol. 145, no. 1, pp. 3–27, 1995.

[12] B. Brady and F. Leighton, "Seismicity anomaly prior to a moderate rock burst: a case study," *International Journal of Rock Mechanics and Mining Sciences and Geomechanics Abstracts*, vol. 14, no. 3, pp. 127–132, 1977.

[13] F. L. Kent, J. S. Coggan, and P. F. R. Altounyan, "Investigation into factors affecting roadway deformation in the Selby coalfield," *Geotechnical and Geological Engineering*, vol. 16, no. 4, pp. 273–289, 1999.

[14] W. S. Phillips, J. T. Rutledge, L. S. House, and M. C. Feher, "Induced microearthquake patterns in hydrocarbon and geothermal reservoirs: six case studies," *Pure and Applied Geophysics*, vol. 159, no. 1, pp. 345–369, 2002.

[15] Y. L. Tan, K. X. He, Z. S. Ma, and X. H. Yan, "Researches on remote monitoring and forecasting system for hard roof fall," *Chinese Journal of Rock Mechanics and Engineering*, vol. 25, no. 8, pp. 1705–1709, 2006, in Chinese.

[16] C. X. Yang, Z. Q. Luo, and L. Z. Tang, "Study on rule of geostatic activity based on microseismic monitoring technique in deep mining," *Chinese Journal of Rock Mechanics and Engineering*, vol. 159, no. 13, pp. 818–824, 2007, in Chinese.

[17] Q. W. Lian, X. M. Song, and T. F. Gu, "The mathematic model of roof unstability and weighting pre-waring in mine and its application," *Journal of Mining & Safety Engineering*, vol. 28, no. 4, pp. 517–523, 2011, in Chinese.

[18] M. C. He, W. L. Gong, H. M. Zhai et al., "Physical modeling of deep ground excavation in geologically horizontal strata based on infrared thermography," *Tunnelling and Underground Space Technology*, vol. 25, no. 4, pp. 366–376, 2010.

[19] W. L. Gong, Y. X. Gong, and A. F. Long, "Multi-filter analysis of infrared images from the excavation experiment in horizontally stratified rocks," *Infrared Physics and Technology*, vol. 56, pp. 57–68, 2013.